CCS 中国化学会 | CHINESE CHEMICAL SOCIETY | ICCAS 1956 | ROYAL SOCIETY OF CHEMISTRY

RESEARCH ARTICLE

Check for updates

Low-cost and LiTFSI-free diphenylamine-substituted hole transporting materials for highly efficient perovskite solar cells and modules†

Shengli Su,‡[a] Pin Lv,‡[a] Min Hu,*[b] Yuxi Zhang,[ac] Huiyu Yin,[a] Yanqing Zhu,[ac] Junye Pan,[a] Yulong Wang,[a] Wangnan Li, [ID] *[d] Yaoguang Rong, [ID] [e] Zhiliang Ku, [ID] [cf] Fuzhi Huang, [ID] [cf] Yi-Bing Cheng[cf] and Jianfeng Lu [ID] *[ac]

To date, the most efficient metal halide perovskite solar cells employ an n–i–p architecture that uses a 2,2,7′,7′-tetrakis(*N*,*N*-di-*p*-methoxyphenylamine)-9,9′-spirobifluorene (spiro-OMeTAD) as the hole-transporting material (HTM), which achieves optimum conductivity with the addition of lithium bis(trifluoromethane)sulfonimide (LiTFSI) and air exposure. However, the instability caused by these additives limits the further development of PSCs toward commercialization. Here, we designed and synthesized a novel HTM, 9-(4-((2-ethylhexyl)oxy)phenyl)-N^2,N^2,N^7,N^7-tetrakis(4-methoxyphenyl)-9*H*-carbazole-2,7-diamine (SC-2), and oxidized SC-2 was synthesized to dope SC-2 to replace the conventionally used spiro-OMeTAD system. The film conductivity, morphology, and solar cells were optimized by varying the doping content. As a result, a champion efficiency of 21.3% under AM 1.5G 1- sun irradiation is achieved, which is one of the best efficiencies of the HTL doped by its pre-oxidized salt. The non-encapsulated cells based on doped SC-2 retained 95% of their initial performance after aging for 1450 h (ISOS-D-1), which is better than those of the cells based on doped spiro-OMeTAD (*ca.* 77%) and doped EH44 (*ca.* 76%). In addition, an efficiency of 14.6% is demonstrated for perovskite solar modules of 5 cm × 5 cm in size using a 10.0 cm² aperture area under AM 1.5G irradiation based on this new HTM.

1. Introduction

In recent years, metal halide perovskite solar cells (PSCs) have been developed rapidly due to the excellent photoelectric properties of perovskite materials. The power conversion efficiency (PCE) of PSCs has exceeded 25%, which is close to that of silicon solar cells.[1–3] PSCs employing a sandwich n–i–p structure consisting of a perovskite active layer between an inorganic electron transporting layer (ETL) and an organic hole transport layer (HTL) often achieve excellent photoelectric properties.[4,5] So far, significant improvements have been made in the efficiency,[6] and the research direction has been turned towards the combination of efficiency and stability recently.[7]

Currently, light (including ultraviolet light),[8] thermal,[9] oxygen,[10] and moisture stability[11] of PSCs are the focus of research. One way to improve the device stability is to optimize the HTL.[12] 2,2′,7,7′-Tetrakis(*N*,*N*-di-*p*-methoxyphenylamine)-9,9′-spirobifluorene (spiro-OMeTAD), which adapts a diphenylamine-based structure, is the most widely used hole-transporting material (HTM) in the PSC field.[13,14] Spiro-OMeTAD has a low hole mobility in its original form due to its propeller-like structure consisting of diphenylamine moieties and the intrinsic arrangement of sp³ hybrid atomic bonds.[13] These structural characteristics result in large distances between molecules and low conductivity and hole mobility,[15] which makes the use of dopants essential. Doping is a main strategy to modulate the conductivity of semiconductors, in which impurities are

[a] *State Key Laboratory of Silicate Materials for Architectures, Wuhan University of Technology, Wuhan 430070, China. E-mail: jianfeng.lu@whut.edu.cn*

[b] *School of Electronic and Electrical Engineering, Hubei Province Engineering Research Center for Intelligent Micro-Nano Medical Equipment and Key Technologies, Wuhan Textile University, Wuhan 430200, China. E-mail: hm@wtu.edu.cn*

[c] *Foshan Xianhu Laboratory of the Advanced Energy Science and Technology Guangdong Laboratory, Foshan 528216, China*

[d] *Hubei Key Laboratory of Low Dimensional Optoelectronic Material and Devices, Hubei University of Arts and Science, Xiangyang 441053, China. E-mail: liwangnan@hbuas.edu.cn*
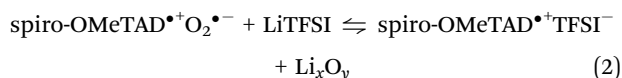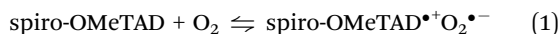
[e] *School of Chemistry, Chemical Engineering and Life Sciences, Wuhan University of Technology, Wuhan 430070, P. R. China*

[f] *State Key Laboratory of Advanced Technology for Materials Synthesis and Processing, Wuhan University of Technology, Wuhan 430070, China*

† Electronic supplementary information (ESI) available. See DOI: https://doi.org/10.1039/d2qm01330d

‡ These authors contributed equally to this work.

introduced into the semiconductor to increase the concentration of charge carriers and improve the conductivity.[16] Usually, lithium bis(trifluoromethane)sulfonimide (LiTFSI) is used as an additive for spiro-OMeTAD or poly(triaryl amine) (PTAA) to improve their conductivity.[17] It can expedite the oxygen-induced oxidation of spiro-OMeTAD as shown in eqn (1) and (2):[15]

$$\text{spiro-OMeTAD} + O_2 \leftrightharpoons \text{spiro-OMeTAD}^{\bullet+}O_2^{\bullet-} \qquad (1)$$

$$\text{spiro-OMeTAD}^{\bullet+}O_2^{\bullet-} + \text{LiTFSI} \leftrightharpoons \text{spiro-OMeTAD}^{\bullet+}\text{TFSI}^-$$
$$+ Li_xO_y \qquad (2)$$

However, the speed of this oxidation reaction is relatively slow, which can significantly affect the reproducibility of the solar cells.[18] Moreover, the hygroscopic LiTFSI can absorb moisture from air and aggregate from the spiro-OMeTAD film, strongly affecting the interfacial energetics and morphology.[19]

Unlike the doping of spiro-OMeTAD with O_2 and LiTFSI, the electrical conductivity of HTLs can be improved by adding its oxidized salt analogue as well.[20,21] Tan *et al.* quantitatively doped spiro-OMeTAD with its oxidized salt (spiro-OMeTAD-(TFSI)$_2$) without using any lithium salts, which improved the HTL conductivity and device efficiency ($\sim$19%).[22] With this strategy, the unwanted intercalation of Li ions into the perovskite active layer is also prevented.[19] Snaith *et al.* implemented this strategy to a low-cost, synthetically simple carbazole-cored HTM, 9-(2-ethylhexyl)-N^2,N^2,N^7,N^7-tetrakis(4-methoxyphenyl)-9H-carbazole-2,7-diamine (EH44).[23] They fabricated efficient PSCs with enhanced water resistance by doping it with its pre-oxidized TFSI$^-$ salt (EH44-ox). Christians *et al.* subsequently used EH44-ox doped EH44 as the HTL to achieve an efficiency of 18.5%.[11] The non-encapsulated solar cells retained 94% of their peak PCE after 1000 hours of continuous operation at ambient condition, demonstrating a promising application of EH44 against moisture. Schloemer *et al.* modulated the diphenylamine pendant substituents of EH44 with fluorene and

carbazole, and doped them with EH44-ox, respectively.[24] The devices demonstrated better stability than the state-of-the-art EH44 as well as the conventional spiro-OMeTAD system. Although advantages in terms of stability have been demonstrated with this doping strategy, *i.e.*, doping an organic HTM with its pre-oxidized salt, the efficiency of solar cells is lower than 20%.

Unlike the previous change of contralateral chain groups, herein we design and synthesize a new HTM, 9-(4-((2-ethylhexyl)oxy)phenyl)-N^2,N^2,N^7,N^7-tetrakis(4-methoxyphenyl)-9H-carbazole-2,7-diamine (SC-2), by introducing a phenoxy group at the nitrogen atom of carbazole core in EH44 to improve the charge transport capacity and molecular rigidity. The morphology, spectral, and electrical properties of HTL films are characterized by using a series of characterizations, such as scanning electronic microscopy (SEM), optical microscopy, photoluminescence (PL) spectroscopy, time-resolved PL (TRPL) spectroscopy, and fluorescence lifetime imaging microscopy (FLIM) techniques. The molecules were applied as a HTM in n–i–p structured PSCs to compare with the traditional spiro-OMeTAD and EH44. The stability of this new HTM was studied by aging the devices at ambient without encapsulation. Moreover, larger area (5 cm × 5 cm) modules were fabricated to study the feasibility of this new material in future commercialization applications.

2. Results and discussion

2.1 Synthesis of HTMs

The structures of spiro-OMeTAD, EH44, and SC-2 are depicted in Fig. 1. The carbazole-based core and diphenylamine groups in SC-2 allow π–π conjugations, while the hydrophobic alkyl chain is to enhance the hydrophobicity of the film, laying a foundation for good stability of the HTL films.[25] The synthesis routes to SC-2 are illustrated in Fig. S1a (ESI†), and the synthetic procedure and full chemical characterization are provided in the ESI.† Briefly, the target compound SC-2 was obtained by the
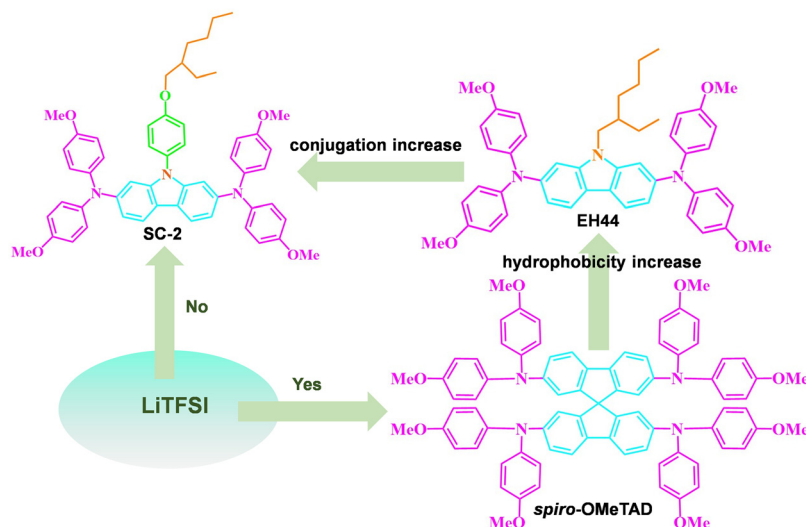

Fig. 1 Chemical structures of spiro-OMeTAD, EH44, and SC-2.

Buchwald–Hartwig coupling reaction of 2,7-dibromo-9-(4-((2-ethyl-hexyl)oxy)phenyl)-9H-carbazole with bis(4-methoxyphenyl)amine catalyzed by palladium. As a contrast, EH44 was synthesized according to the literature report.[26] The target products are fully confirmed by nuclear magnetic resonance (NMR) and high resolution mass spectrometry (HRMS). SC-2 is well soluble in commonly used organic solvents, such as chloroform, chlorobenzene, and ethyl acetate. We list the cost for the synthesis of SC-2, which is much lower than that of spiro-OMeTAD (Table S1, ESI†). The SC-2 powder and AgTFSI are dissolved in dichloromethane for the oxidation reaction to obtain its oxidized TFSI⁻ salt analogue (SC-2-ox), as shown in Fig. S1b (ESI†), and the product is purified by recrystallization as we describe in the Experimental Section.

2.2 Spectroscopy and electrical properties

Fig. 2a shows the UV-Vis absorption spectra of EH44, EH44-ox and SC-2, SC-2-ox in chloroform solution. SC-2 has the most intensive absorption peak at 393 nm, while it is 389 nm for EH44. The oxidized salts of SC-2 and EH44 show strong absorption in the near IR. The absorption and fluorescence emission of SC-2 and EH44 thin films are displayed in Fig. S2a (ESI†). In the PL spectra, SC-2 demonstrates the maximum emission peak at 428 nm, whereas EH44 has a strong peak at 422 nm. Both the absorption and emission of SC-2 are red-shifted in comparison with EH44, which is due to the expanded conjugation effect of the extra benzene ring.[27] The absorption onsets of SC-2 and EH44 are 424 and 421 nm, which indicate the estimated optical bandgaps (E_g) of 2.98 and 2.99 eV, respectively.

The spiro-OMeTAD film has an absorption peak at 382 nm and a fluorescence emission peak at 428 nm as shown in Fig. S2b (ESI†), which are consistent with previous reports.[14]

Cyclic voltammetry (CV) was performed to determine the oxidation potentials and energy levels of the HTMs.[28] This is crucial to determine the possible applicability in PSCs. CV was performed in chlorobenzene at room temperature and tetra-butylammonium hexafluorophosphate (0.1 mol L⁻¹) was used as the supporting electrolyte. All potentials are internally referenced to the ferrocene/ferricenium (Fc/Fc⁺) redox pair. Half-wave potentials ($E_{1/2}$) were calculated from the cathodic and anodic peak potentials. Highest occupied molecular orbital (HOMO) energy levels are determined by the onset values of the oxidation potential ($E_{1/2} + E_{HOMO} = -4.8$ eV), whereby the lowest unoccupied molecular orbital (LUMO) energy levels are calculated from the HOMO energy and the optical gap.[29] The data are summarized in Table 1 and Fig. 2b. The HOMO energy levels of pristine spiro-OMeTAD, EH44, and SC-2 are −5.07, −4.76, and −4.78 eV, respectively.

The thermal behaviors of HTMs were determined by thermo-gravimetric analysis (TGA) and differential scanning calorimetry (DSC) measurements (Fig. 2c and Fig. S3, ESI†). Both molecules display good thermal stability, showing 5% weight loss at 400 and 416 °C for EH44 and SC-2, respectively. DSC scans demonstrate that EH44 and SC-2 are naturally in amorphous phases, showing a higher glass transition temperature (T_g) of the latter (EH44: 44 °C vs. SC-2: 49 °C) but much lower than the state of the art of spiro-OMeTAD (154 °C for pristine form and 91 °C after doped by LiTFSI/tBP/cobalt complex).[30]
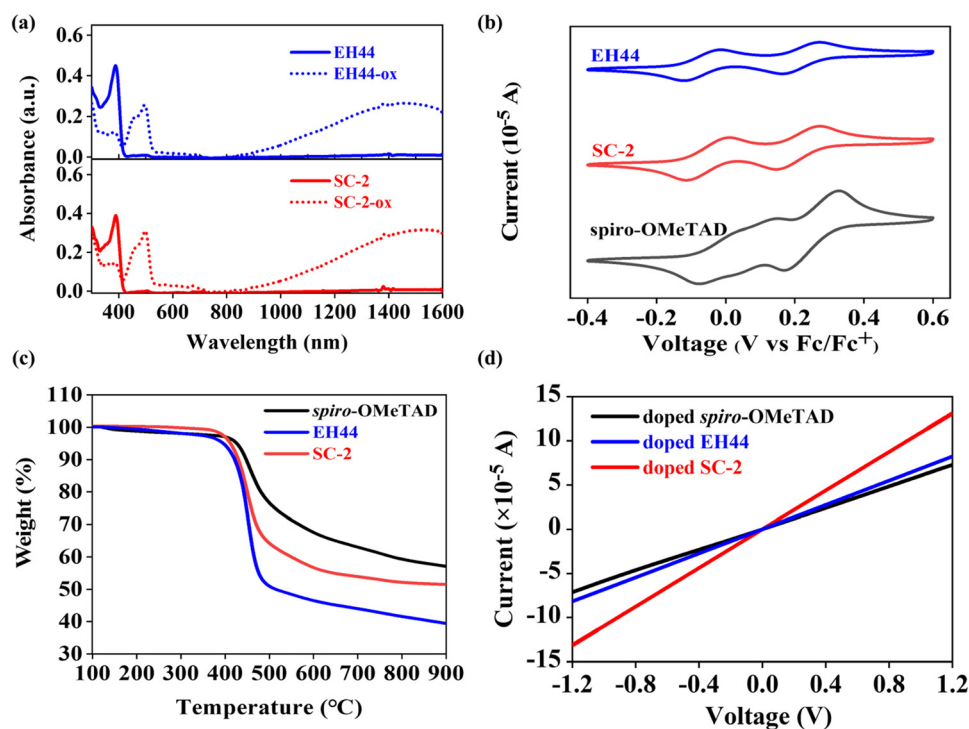

Fig. 2 (a) UV-Vis absorption spectra of EH44, EH44-ox and SC-2, SC-ox in chloroform. (b) CV of pristine spiro-OMeTAD, EH44, and pristine SC-2. (c) TGA curves of spiro-OMeTAD, EH44, and SC-2. (d) I–V curves of doped spiro-OMeTAD, doped EH44, and doped SC-2 films.

Table 1 Detailed optoelectronic properties of spiro-OMeTAD, SC-2, and EH44

HTMs	$\lambda_{abs,max}$ (nm) Solution	$\lambda_{abs,max}$ (nm) Film	$\lambda_{emi,max}$ (nm) Film	E_g (eV)	E_{HOMO} (eV)	Conductivity (S cm^{-1}) Pristine	Doped
spiro-OMeTAD	380	382	428	2.97	−5.07	2.86×10^{-7}	6.08×10^{-5}
EH44	389	393	422	2.99	−4.76	6.71×10^{-6}	6.80×10^{-5}
SC-2	393	397	428	2.98	−4.78	1.23×10^{-5}	1.09×10^{-4}

The T_g values of SC-2-ox and SC-2-ox doped SC-2 (doping level: 15.5 mol%) are 53 and 50 °C. It is interesting to note that the T_g remains almost constant after p-doping, which is different from the behavior of spiro-OMeTAD. These results indicate that SC-2 possesses better thermal stability than the EH44 counterpart.[31]

The conductivity of different HTL films was measured using interdigitated gold microelectrode arrays (IDAs, Fig. S4a, ESI†).[32] The conductivity of the doped HTL films is shown in Fig. 2d and the pristine HTL films is shown in Fig. S4b (ESI†). We plotted the I–V curves of SC-2 with different doping levels in Fig. S4c (ESI†), and the calculated electrical conductivity values are plotted in Fig. S4d (ESI†). The conductivity of the pristine SC-2 film is 1.23×10^{-5} S cm^{-1}, and reaches the maximum of 1.09×10^{-4} S cm^{-1} when doped with 15.5 mol% SC-2-ox. Further increasing the content of SC-2-ox leads to a decrease in the conductivity, showing 7.67×10^{-5} S cm^{-1} when the doping level is 25.5 mol%. The conductivity of the pristine spiro-OMeTAD film is 2.86×10^{-7} S cm^{-1}, and a doped spiro-OMeTAD (LiTFSI/tBP/cobalt complex) is 6.08×10^{-5} S cm^{-1}, which is consistent with previous results.[14] The conductivity of the pristine EH44 film is 6.71×10^{-6} S cm^{-1}, and 6.80×10^{-5} S cm^{-1} for the EH44-ox doped film. Overall, the conductivity of doped SC-2 is higher than that of doped spiro-OMeTAD and doped EH44.

The morphology of the HTL film is important to the performance of solar cells due to its significant influence on hole extraction and charge recombination processes.[1] XRD analysis confirmed the formation of the target crystal structure of $FA_{0.92}MA_{0.08}PbI_{2.76}Br_{0.24}$ (FA = formamidinium, MA = methylammonium) perovskites and no negative effect on the perovskite crystal with the HTL deposition (Fig. S5, ESI†). The top view SEM images of the perovskite films are shown in Fig. 3a, showing a uniform and compact morphology as expected. After deposition of HTLs, i.e. doped spiro-OMeTAD, doped EH44, and doped SC-2, all samples exhibit uniform and complete coverage on the perovskite layer (Fig. 3b–d). It is noticed that the films based on SC-2 and EH44 show a more uniform and less aggregations in optical microscopy images (Fig. S6a–d, ESI†), which is possibly due to the absence of LiTFSI in the film.[22]

Ultraviolet photoelectron spectroscopy (UPS) was performed to estimate the band alignment of the doped SC-2 film. As shown in Fig. 3e, the photoemission onset and cut-off are 1.54 and 17.59 eV, corresponding to a valence band maximum (VBM) of −5.17 eV calculated by the formula shown in Fig. 3f, which demonstrates the successful p-doping of SC-2 after the addition of SC-2-ox. This value is more positive than the valence band edge of the $FA_{0.92}MA_{0.08}PbI_{2.76}Br_{0.24}$ perovskite (5.95 eV).[33] The energy diagrams of doped SC-2, perovskite, and SnO$_2$ are shown in Fig. 3g. The figure shows that the valence band of the doped SC-2 film matches well with the perovskite.
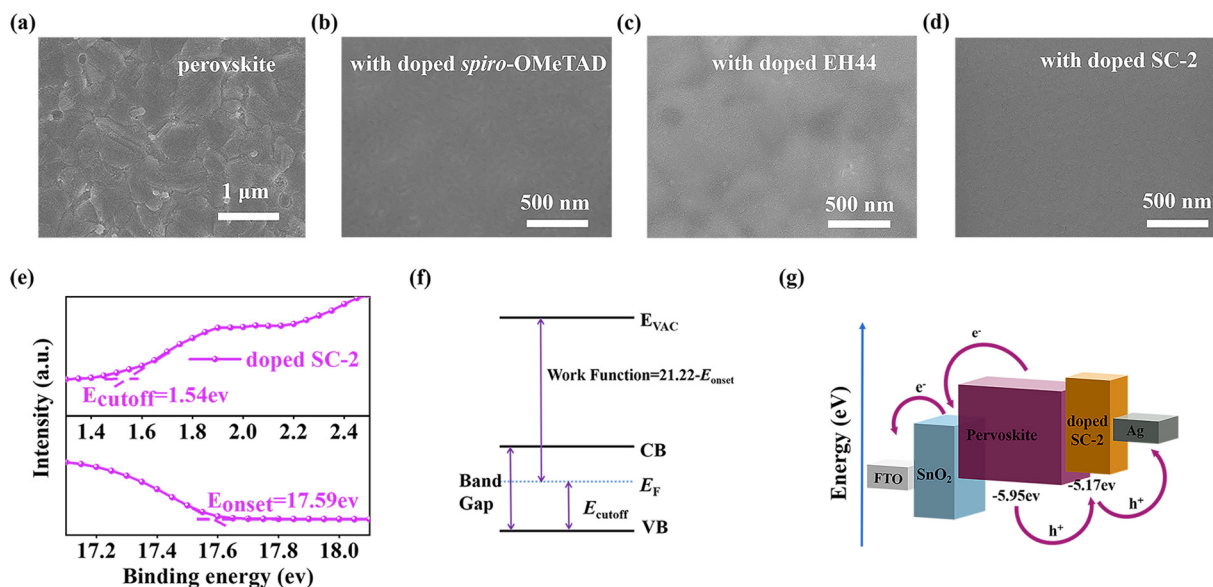

Fig. 3 SEM images of the (a) $FA_{0.92}MA_{0.08}PbI_{2.76}Br_{0.24}$ perovskite, and perovskite covered with (b) doped spiro-OMeTAD, (c) doped EH44, and (d) doped SC-2. (e) UPS of the doped SC-2 film. (f) Energy band diagram of the doped SC-2 film in UPS measurement. (g) Schematic illustration of the energy level diagram of each layer in PSCs. The sample structure in SEM and UPS measurement is FTO|SnO$_2$|$FA_{0.92}MA_{0.08}PbI_{2.76}Br_{0.24}$|HTL.

2.3 Photovoltaic performance

To evaluate the potential of SC-2 in solar cell application, typical n–i–p PSCs with an architecture of FTO|SnO$_2$|FA$_{0.92}$-MA$_{0.08}$PbI$_{2.76}$Br$_{0.24}$|HTL|MoO$_x$|Ag were fabricated (Fig. 4a). The SnO$_2$ film is deposited by chemical bath deposition with a thickness of $\sim$20 nm.[34] The perovskite is deposited according to a previous report with a thickness of 600 nm (see cross-sectional SEM images in Fig. 4b and Fig. S7, ESI†).[35] The thickness of the doped SC-2 layer is $\sim$110 nm, while it is $\sim$220 nm for the doped spiro-OMeTAD. Ag is used as the counter electrode to reduce the production cost. A thin layer of MoO$_x$ (ca. 5 nm) is inserted between the HTL and Ag to prevent the penetration of Ag into the perovskite layer, which has been demonstrated to be detrimental to the stability of PSCs.[27] We first studied the performance of the solar cells with HTLs based on different doping levels. The efficiency reaches the highest value when the doping level is 15.5 mol%, which is consistent with the trend of conductivity. A further increase of the doping level results in a decrease of the solar cell performance, showing a best efficiency of 18.0% when it is 25.5 mol% (Fig. S8 and Table S2, ESI†).

Current density–voltage (J–V) curves of the champion solar cells based on three HTLs are shown in Fig. 4c. The devices based on doped spiro-OMeTAD show the best PCE of 21.8%, with an open-circuit voltage (V_{OC}) of 1.15 V, a short-circuit current density (J_{SC}) of 24.5 mA cm^{-2}, and a fill factor (FF) of 0.79, which demonstrate good quality of solar cells in this study.[36] The devices based on doped EH44 shows the highest PCE of 18.9%, with a V_{OC} of 1.04 V, a J_{SC} of 24.5 mA cm^{-2} and a FF of 0.74, which is consistent with previous reports.[11] Under similar conditions, the best-performing device based on doped SC-2 shows a V_{OC} of 1.12 V, a J_{SC} of 25.1 mA cm^{-2} and a FF of 0.75, yielding a PCE of 21.3%. To the best of our knowledge, this is one of the best efficiencies when the HTL is doped with its pre-oxidized salt. As shown in Fig. 4d, the Quasi-stabilized power output (q-SPO) values are 21.4, 17.8, and 20.0% for the champion PSCs based on doped spiro-OMeTAD, doped EH44, and doped SC-2, respectively, which are consistent with the values obtained from the J–V characteristics. External quantum efficiency (EQE) spectra and the corresponding integrated J_{SC} values are shown in Fig. 4e. The integrated J_{SC} values are 22.5, 22.7, and 22.9 mA cm^{-2} for the champion PSCs, which agree well with the values obtained from J–V characteristics.

The efficiency histograms of the cells based on different HTMs are depicted in Fig. 4f, while the other photovoltaic parameters (V_{OC}, J_{SC}, and FF) are presented in Fig. S9a–c, ESI† and Table 2. The average PCEs for PSCs based on doped spiro-OMeTAD, doped EH44, and doped SC-2 were 21.3 $\pm$ 0.5, 18.4 $\pm$ 0.5, and 20.5 $\pm$ 0.8%, respectively. The average efficiencies follow a similar trend of the best-performing cells, which demonstrates good reproducibility. The doped SC-2 devices exhibit a slightly higher J_{SC} and FF, and a significantly higher V_{OC} as compared to the devices based on doped EH44. Since the additional benzene ring in SC-2 increases the conjugation effect and thus the conductivity of the film,[37] this superior performance can be explained by the chemical nature of SC-2. In addition, the isooctyloxy group in SC-2 can act as the Lewis site, which is reported to be able to interact with adjacent perovskites and improve the contact between the active layer and HTL.[38]
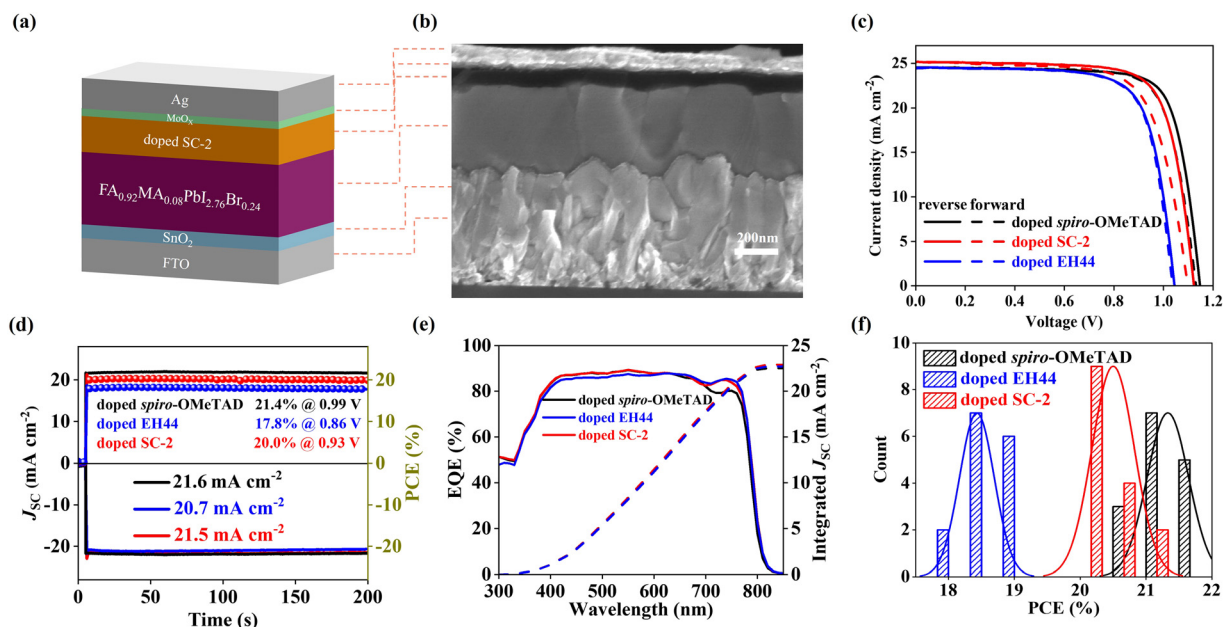

Fig. 4 (a) Schematic diagram of a typical n–i–p PSC with an architecture of FTO|SnO$_2$|perovskite|HTL|MoO$_x$|Ag. (b) SEM images of the best-performing PSCs based on doped SC-2. (c) J–V curves of (d) q-SPO at a fixed bias around the maximum power point. (e) EQE spectra and corresponding integrated current densities. (f) The efficiency histograms of 15 independent cells based on different HTLs. All photovoltaic parameters are obtained under AM 1.5G 1 sun irradiation with a mask area of 0.16 cm^2.

Table 2 Photovoltaic parameters[a] of PSCs based on different HTLs under AM 1.5G 1 sun simulated irradiation (mask area: 0.16 cm^2)

HTL			V_{OC} (V)	J_{SC} (mA cm^{-2})	FF	PCE (%)
Doped spiro-OMeTAD	Average[b]		1.13 ± 0.02	24.3 ± 0.2	0.78 ± 0.01	21.3 ± 0.5
	Best[c]	FB to SC	1.15	24.5	0.77	21.8
		SC to FB	1.13	24.5	0.76	21.1
Doped EH44	Average		1.03 ± 0.01	24.2 ± 0.3	0.74 ± 0.01	18.4 ± 0.5
	Best	FB to SC	1.04	24.5	0.74	18.9
		SC to FB	1.04	24.4	0.74	18.8
Doped SC-2	Best	Average	1.10 ± 0.02	24.8 ± 0.4	0.75 ± 0.01	20.5 ± 0.8
		FB to SC	1.12	25.1	0.75	21.3
		SC to FB	1.10	25.2	0.71	19.7

[a] V_{OC}, J_{SC}, FF and PCE data are derived from the J–V curves. [b] The average parameters are extracted from recording 15 independent devices of each type in the scan direction of forward-bias (FB) to short-circuit (SC). [c] The best-performing devices recorded in both directions.

To study the charge transfer between the perovskite layer and HTL, FLIM was performed (Fig. 5a–c and Fig. S10, ESI†).[39] A significantly decreased PL lifetime and smaller signal range were observed after coating the doped EH44, and these effects were even further enhanced for doped spiro-OMeTAD (Fig. S10, ESI†) and doped SC-2. To further study the charge transfer dynamics, steady-state PL spectra of perovskite covered with different HTLs were recorded. All examined samples display similar PL spectral profiles with a maximum at 780 nm (Fig. 5d), while the intensity of the perovskite film is significantly quenched with approximately 98%, 92%, and 95% of its initial value by doped spiro-OMeTAD, doped EH44, and doped SC-2 films, respectively. The large quenched values suggest an efficient charge transfer from the perovskite to all HTLs. The TRPL spectra (Fig. 5e) were quantitatively fitted by a bi-exponential function following eqn (3):[40]

$$I(t) = I_0 + A_1 \exp(-t/\tau_1) + A_2 \exp(-t/\tau_2) \tag{3}$$

where τ_1 and τ_2 represent the fast and slow attenuation component, respectively. The average carrier lifetime (τ_{ave}) of the perovskite film is 1773.9 ns, indicating the good quality of the film. When coated with doped spiro-OMeTAD, doped EH44, and doped SC-2 HTLs, the lifetime sharply reduced to 94.1, 166.8, and 140.8 ns, which is consistent with the steady state PL study. The shorter TRPL lifetime of samples based on doped SC-2 in comparison with the EH44 indicates a faster charge transfer from the perovskite to HTL (Table S3, ESI†). On the other hand, the TRPL lifetime of the perovskite covered with doped spiro-OMeTAD is shorter that with doped SC-2, which indicates a slower charge transfer from the perovskite to the latter. This should be the reason for the lower device performance in Table 2. Overall, PL characterizations consistently attest the improved charge-extraction capacity of the doped SC-2 in comparison with doped EH44.

The built in potential (V_{bi}) is important for maximizing the performance of a solar cell, offering the beneficial properties of
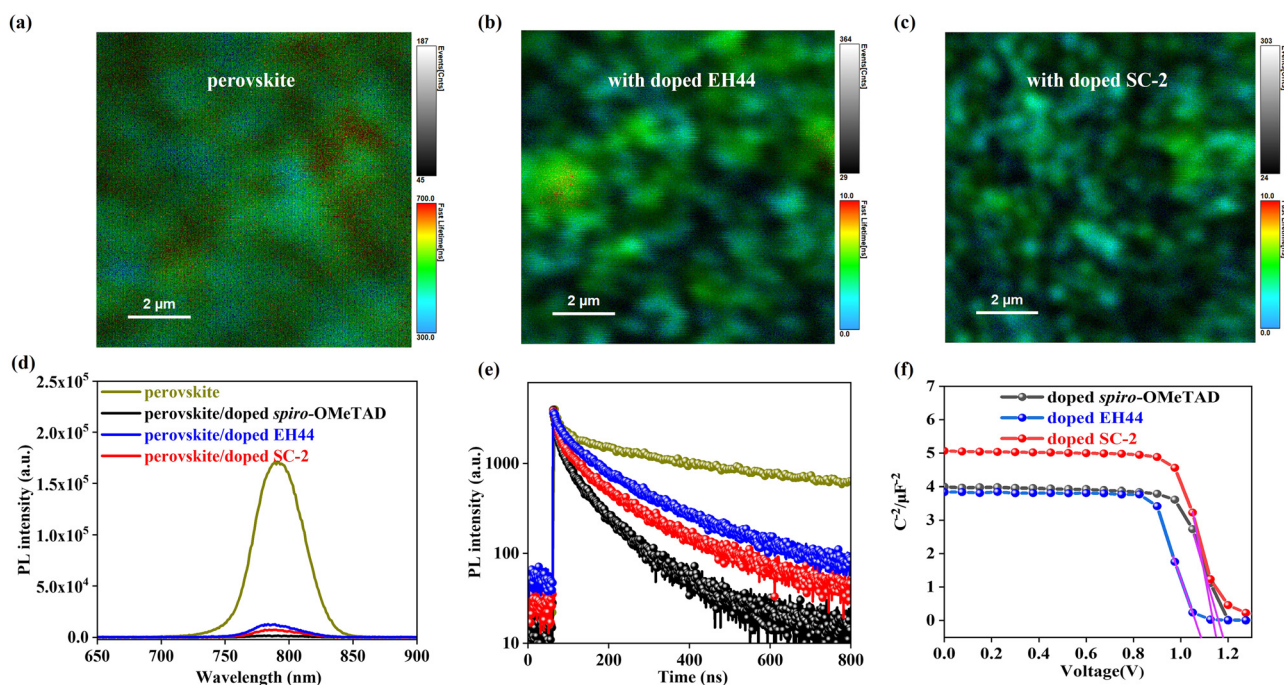

Fig. 5 FLIM images of the (a) perovskite and perovskite covered with (b) doped EH44, and (c) doped SC-2. (d) Steady-state PL spectra, and (e) TRPL spectra of the perovskite w/o HTL covering. The sample structure is glass|perovskite|HTL. (f) Mott–Schottky plots of solar cells.

charge selectivity and reducing recombination. By plotting the capacitance–voltage (C–V) curve with Mott–Schottky analysis, the V_{bi} can be extracted by eqn (4):

$$\frac{1}{C^2} = \frac{2(V_{bi} - V)}{A^2 e \varepsilon_0 N_A} \qquad (4)$$

where C is the capacitance under applied voltage, and A, e, ε_0, ε and N_A are the device area, elementary charge, vacuum dielectric constant, relative dielectric constant of the perovskite and carrier concentration, respectively. As shown in Fig. 5f, the V_{bi} values are 1.17, 1.08 and 1.15 V for the devices based on doped spiro-OMeTAD, doped EH44, and doped SC-2, respectively. According to Ravishankar's report,[41] a higher V_{OC} value always results in a larger V_{bi} due to a fundamental dependence of the recombination resistance of the perovskite layer on its V_{OC} in combination with charge injection or multilayer-capacitance transitions. In consideration of an identical device architecture and functional layers except for HTL, the higher V_{OC} and V_{bi} values of doped SC-2 devices in comparison with that of doped EH44 is due to an enhanced charge selectivity and reduced recombination.

2.4 Stability studies

The stability of solar cells was first evaluated by aging them at 25 ± 5 °C with a relative humidity (RH) of $35 \pm 5\%$ without encapsulation (Fig. 6a). The devices based on doped SC-2 maintained 95% of their initial PCEs after 1450 h, while it is 77% and 76% for the PSCs based on doped spiro-OMeTAD and doped EH44, respectively. The corresponding photovoltaic parameters (V_{OC}, J_{SC}, and FF) are presented in Fig. S11a–c (ESI†). This result suggests that the doped SC-2-based devices are more tolerant to moisture and oxygen than the conventional doped spiro-OMeTAD at room temperature. The moisture stability of the HTLs has been investigated by aging them in a high humidity ($75 \pm 5\%$) environment. Fig. S12 (ESI†) demonstrates a more robust morphology of doped SC-2 at higher humidity in comparison with doped spiro-OMeTAD. The water contact angles for HTLs based on doped spiro-OMeTAD, doped EH44, and doped SC-2 are 94.5, 98.0, and 102.5°, respectively (Fig. 6b). The larger contact angle of doped SC-2 suggests that it is more hydrophobic than the other two, which is one of the reasons for the better stability of the corresponding solar cells. After aging under the atmosphere, the contact angles are reduced to 88.7, 92.5, and 102.2° for the doped spiro-OMeTAD, doped EH44, and doped SC-2 films, respectively (Fig. 6b). It is noticed that the contact angle of doped SC-2 decreases less than the other two in comparison with that after aging. In addition, the absorption spectra of non-encapsulated FTO|SnO$_2$|perovskite covered with the doped SC-2 film remain almost unchanged after aging for 21 days, whereas a continuous reduction in the absorption intensity is observed for the doped spiro-OMeTAD and doped EH44 samples (Fig. 6c and 6d). These results explain the enhanced stability of the solar cells based on doped SC-2. Previous reports
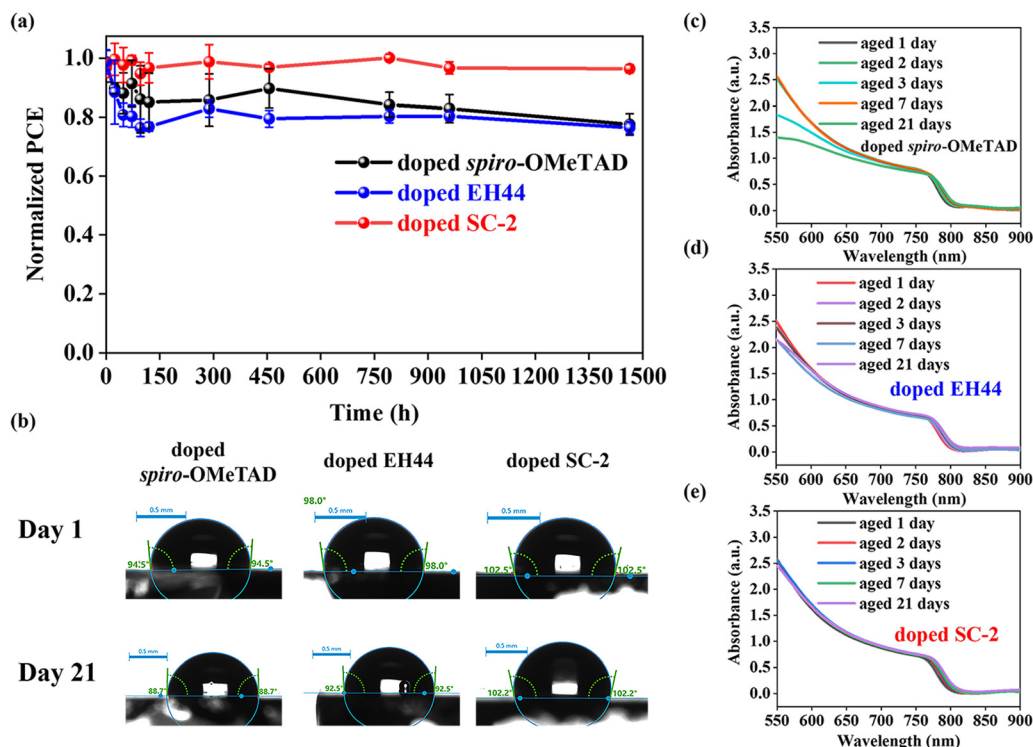

Fig. 6 (a) Evolution of normalized PCE for non-encapsulated solar cells aged at a temperature of 25 ± 5 °C and RH of $25 \pm 5\%$ in the dark. (b) Water contact angle images of HTLs. The sample structure is FTO|SnO$_2$|perovskite|HTLs. UV-Vis spectra of non-encapsulated FTO|SnO$_2$|perovskite covered with (c) doped spiro-OMeTAD, (d) doped EH44, and (e) doped SC-2 films under ambient conditions with a relative humidity of $25 \pm 5\%$ and temperature of 25 ± 5 °C.
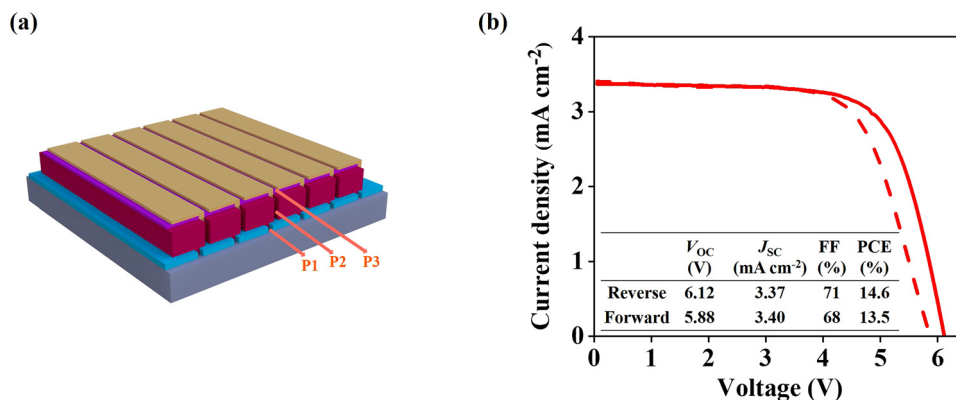
Fig. 7 (a) Schematic diagram of a FTO|SnO$_2$|perovskite|HTL|Au perovskite solar module (full size: 5 cm × 5 cm, with 6 series-connected sub-cells). (b) *J–V* curve of the best-performing module under AM 1.5G 1 sun irradiation based on spin-coated perovskite and doped SC-2 HTL with a mask area of 10.0 cm^2.

have demonstrated that long alkyl chains can effectively resist moisture invasion.[42] Therefore, the enhanced moisture resistance is referred to the additional alkyl chain in SC-2 and elimination of LiTFSI.[43] In addition, the performance of solar cells aged at a higher temperature (55 ± 5 °C) has been studied. As seen in Fig. S13 (ESI†), after aging at 55 ± 5 °C in air without encapsulation for 7 hours, the PCE of the cell based on doped SC-2 decreased more compared to the doped spiro-OMeTAD cell, which is due to lower T_g as illustrated in Fig. S3 (ESI†). Several studies have been reported to improve the thermal stability of small molecules based HTLs.[44–46] For example, Wang *et al.* reported that mixing spiro-OMeTAD with thermally stable polymer poly(9-vinylcarbazole) can substantially improve its thermal stability.[45] Therefore, we assume that this could be a method to improve the thermal stability of SC-2.

2.5 Large area perovskite solar modules

Moreover, we fabricated larger area (substrate size: 5 cm × 5 cm, active area: 10.0 cm^2) perovskite solar modules (Fig. 7a, six series-connected sub-cells) with doped SC-2 to demonstrate the scalability of this new system. The doped SC-2 is deposited on large area perovskite film with a size of 5 cm × 5 cm following the procedures developed by our group.[43] As shown in Fig. 7b, a champion PCE of 14.6% (with a mask area of 10.0 cm^2) was achieved, which demonstrates a promising step forward in the development of large-scale perovskite photovoltaics with stable and low-cost HTM.

3. Conclusion

We conclude by emphasizing that the oxidized form of organic HTMs can be synthesized and used as the p-dopant to enhance the thin film conductivity through judicious molecular design. This advantage means that this method can be used to replace the commonly used hygroscopic LiTFSI, thus guaranteeing both high efficiency and stability when applied in solar cells. As a promising example, we have shown that a diphenylamine-substituted molecule, SC-2, can be used as an efficient and

stable HTL in PSCs. With this HTL, a solar cell with an efficiency of 21.3% has been achieved, which is comparable to that of the conventionally doped spiro-OMeTAD and much higher than the devices based on the state of the art EH44. A series of physical and chemical characterization methods demonstrate that the HTLs based on SC-2 have better charge extraction from the light absorber perovskite layer. Moreover, solar cells based on SC-2 show improved stability against moisture and oxygen, which is primarily due to the enhanced moisture resistance.

Author contributions

Conceptualization: J. L. and S. S.; resources: J. L.; data curation: S. S., P. L., Y. Z., H. Y., Y. Z., J. P., Y. W., and. W. L.; investigation: S. S., M. H., W. L., and J. L.; methodology: J. L. and S. S.; project administration: M. H. and J. L.; writing – original draft: S. S. and J. L.; writing – review & editing: F. H., Y. R., Z. K., and Y. B. C.; supervision: M. H., W. L., and J. L.; funding acquisition: M. H., and J. L.

Conflicts of interest

The authors declare no competing financial interest.

Acknowledgements

References

1 J. Lu and F. Huang, Charge-carrying films for solar cells made quickly and cleanly, *Nature*, 2021, **594**, 27–28.

2 J. Park, J. Kim, H.-S. Yun, M. J. Paik, E. Noh, H. J. Mun, M. G. Kim, T. J. Shin and S. I. Seok, Controlled growth of perovskite layers with volatile alkylammonium chlorides, *Nature*, 2023, DOI: **10.1038/s41586-023-05825-y**.

3 Y. Wang, C. Duan, P. Lv, Z. Ku, J. Lu, F. Huang and Y.-B. Cheng, Printing strategies for scaling-up perovskite solar cells, *Natl. Sci. Rev.*, 2021, **8**, nwab075.

4 Y. Zhu, M. Hu, M. Xu, B. Zhang, F. Huang, Y.-B. Cheng and J. Lu, Bilayer metal halide perovskite for efficient and stable solar cells and modules, *Mater. Futures*, 2022, **1**, 042102.

5 E. H. Jung, N. J. Jeon, E. Y. Park, C. S. Moon, T. J. Shin, T.-Y. Yang, J. H. Noh and J. Seo, Efficient, stable and scalable perovskite solar cells using poly(3-hexylthiophene), *Nature*, 2019, **567**, 511–515.

6 J. Y. Kim, J.-W. Lee, H. S. Jung, H. Shin and N.-G. Park, High-Efficiency Perovskite Solar Cells, *Chem. Rev.*, 2020, **120**, 7867–7918.

7 Y. Cheng and L. Ding, Pushing commercialization of perovskite solar cells by improving their intrinsic stability, *Energy Environ. Sci.*, 2021, **14**, 3233–3255.

8 D. Bryant, N. Aristidou, S. Pont, I. Sanchez-Molina, T. Chotchunangatchaval, S. Wheeler, J. R. Durrant and S. A. Haque, Light and oxygen induced degradation limits the operational stability of methylammonium lead triiodide perovskite solar cells, *Energy Environ. Sci.*, 2016, **9**, 1655–1660.

9 M. Hossain, R. Garai, R. K. Gupta, R. N. Arunagirinathan and P. K. Iyer, Fluoroarene derivative based passivation of perovskite solar cells exhibiting excellent ambient and thermo-stability achieving efficiency >20%, *J. Mater. Chem. C*, 2021, **9**, 10406–10413.

10 N. Aristidou, C. Eames, I. Sanchez-Molina, X. Bu, J. Kosco, M. S. Islam and S. A. Haque, Fast oxygen diffusion and iodide defects mediate oxygen-induced degradation of perovskite solar cells, *Nat. Commun.*, 2017, **8**, 15218.

11 J. A. Christians, P. Schulz, J. S. Tinkham, T. H. Schloemer, S. P. Harvey, B. J. Tremolet de Villers, A. Sellinger, J. J. Berry and J. M. Luther, Tailored interfaces of unencapsulated perovskite solar cells for >1,000 hour operational stability, *Nat. Energy*, 2018, **3**, 68–74.

12 G. Sathiyan, A. A. Syed, C. Chen, C. Wu, L. Tao, X. Ding, Y. Miao, G. Li, M. Cheng and L. Ding, Dual effective dopant based hole transport layer for stable and efficient perovskite solar cells, *Nano Energy*, 2020, **72**, 104673.

13 T. P. I. Saragi, T. Spehr, A. Siebert, T. Fuhrmann-Lieker and J. Salbeck, Spiro Compounds for Organic Optoelectronics, *Chem. Rev.*, 2007, **107**, 1011–1065.

14 Y. Zhang, B. Huang, M. Hu, B. Tan, F. Huang, Y.-B. Cheng, A. N. Simonov and J. Lu, Radical doped hole transporting material for high-efficiency and thermostable perovskite solar cells, *J. Mater. Chem. A*, 2022, **10**, 10604–10613.

15 A. Abate, T. Leijtens, S. Pathak, J. Teuscher, R. Avolio, M. E. Errico, J. Kirkpatrik, J. M. Ball, P. Docampo, I. McPherson and H. J. Snaith, Lithium salts as "redox active" p-type dopants for organic semiconductors and their impact in solid-state dye-sensitized solar cells, *Phys. Chem. Chem. Phys.*, 2013, **15**, 2572–2579.

16 I. Salzmann, G. Heimel, M. Oehzelt, S. Winkler and N. Koch, Molecular Electrical Doping of Organic Semiconductors: Fundamental Mechanisms and Emerging Dopant Design Rules, *Acc. Chem. Res.*, 2016, **49**, 370–378.

17 Z. Hawash, L. K. Ono and Y. Qi, Moisture and Oxygen Enhance Conductivity of LiTFSI-Doped Spiro-MeOTAD Hole Transport Layer in Perovskite Solar Cells, *Adv. Mater. Interfaces*, 2016, **3**, 1600117.

18 B. Tan, S. R. Raga, K. J. Rietwyk, J. Lu, S. O. Fürer, J. C. Griffith, Y.-B. Cheng and U. Bach, The impact of spiro-OMeTAD photodoping on the reversible light-induced transients of perovskite solar cells, *Nano Energy*, 2021, **82**, 105658.

19 J. Kong, Y. Shin, J. A. Röhr, H. Wang, J. Meng, Y. Wu, A. Katzenberg, G. Kim, D. Y. Kim, T.-D. Li, E. Chau, F. Antonio, T. Siboonruang, S. Kwon, K. Lee, J. R. Kim, M. A. Modestino, H. Wang and A. D. Taylor, CO$_2$ doping of organic interlayers for perovskite solar cells, *Nature*, 2021, **594**, 51–56.

20 W. Zhang, F. Zhang, B. Xu, Y. Li, L. Wang, B. Zhang, Y. Guo, J. M. Gardner, L. Sun and L. Kloo, Organic Salts as p-Type Dopants for Efficient LiTFSI-Free Perovskite Solar Cells, *ACS Appl. Mater. Interfaces*, 2020, **12**, 33751–33758.

21 J. Zhang, B. Xu, L. Yang, A. Mingorance, C. Ruan, Y. Hua, L. Wang, N. Vlachopoulos, M. Lira-Cantú, G. Boschloo, A. Hagfeldt, L. Sun and E. M. J. Johansson, Incorporation of counter Ions in organic molecules: new strategy in developing dopant-free hole transport materials for efficient mixed-ion perovskite solar cells, *Adv. Energy Mater.*, 2017, **7**, 1602736.

22 B. Tan, S. R. Raga, A. S. R. Chesman, S. O. Fürer, F. Zheng, D. P. McMeekin, L. Jiang, W. Mao, X. Lin, X. Wen, J. Lu, Y.-B. Cheng and U. Bach, LiTFSI-free spiro-OMeTAD-based perovskite solar cells with power conversion efficiencies exceeding 19%, *Adv. Energy Mater.*, 2019, **9**, 1901519.

23 T. Leijtens, T. Giovenzana, S. N. Habisreutinger, J. S. Tinkham, N. K. Noel, B. A. Kamino, G. Sadoughi, A. Sellinger and H. J. Snaith, Hydrophobic organic hole transporters for improved moisture resistance in metal halide perovskite solar cells, *ACS Appl. Mater. Interfaces*, 2016, **8**, 5981–5989.

24 T. H. Schloemer, T. S. Gehan, J. A. Christians, D. G. Mitchell, A. Dixon, Z. Li, K. Zhu, J. J. Berry, J. M. Luther and A. Sellinger, Thermally stable perovskite solar cells by systematic molecular design of the hole-transport layer, *ACS Energy Lett.*, 2019, **4**, 473–482.

25 X. Jiang, J. Zhang, Y. Liu, Z. Wang, X. Liu, X. Guo and C. Li, Dopant-free polymer/2D/3D perovskite solar cells with high stability, *Nano Energy*, 2021, **90**, 106521.

26 J. Zhang, L. J. Xu, P. Huang, Y. Zhou, Y. Y. Zhu, N. Y. Yuan, J. N. Ding, Z. G. Zhang and Y. F. Li, A simple and dopant-free hole-transporting material based on (2-ethylhexyl)-9H-carbazole

for efficient planar perovskite solar cells, *J. Mater. Chem. C*, 2017, **5**, 12752–12757.

27 T. Niu, W. Zhu, Y. Zhang, Q. Xue, X. Jiao, Z. Wang, Y.-M. Xie, P. Li, R. Chen, F. Huang, Y. Li, H.-L. Yip and Y. Cao, D-A-π-A-D-type Dopant-free Hole Transport Material for Low-Cost, Efficient, and Stable Perovskite Solar Cells, *Joule*, 2021, **5**, 249–269.

28 N. J. Jeon, H. Na, E. H. Jung, T.-Y. Yang, Y. G. Lee, G. Kim, H.-W. Shin, S. Il Seok, J. Lee and J. Seo, A fluorene-terminated hole-transporting material for highly efficient and stable perovskite solar cells, *Nat. Energy*, 2018, **3**, 682–689.

29 Y. Mao, M. Head-Gordon and Y. Shao, Unraveling substituent effects on frontier orbitals of conjugated molecules using an absolutely localized molecular orbital based analysis, *Chem. Sci.*, 2018, **9**, 8598–8607.

30 J.-Y. Seo, H.-S. Kim, S. Akin, M. Stojanovic, E. Simon, M. Fleischer, A. Hagfeldt, S. M. Zakeeruddin and M. Grätzel, Novel p-dopant toward highly efficient and stable perovskite solar cells, *Energy Environ. Sci.*, 2018, **11**, 2985–2992.

31 H. Zhang, H. Xiao, F. Liu, F. Huo, Y. He, Z. Chen, X. Liu, S. Bo, L. Qiu and Z. Zhen, Synthesis of novel nonlinear optical chromophores: achieving enhanced electro-optic activity and thermal stability by introducing rigid steric hindrance groups into the julolidine donor, *J. Mater. Chem. C*, 2017, **5**, 1675–1684.

32 X. Lin, A. N. Jumabekov, N. N. Lal, A. R. Pascoe, D. E. Gómez, N. W. Duffy, A. S. R. Chesman, K. Sears, M. Fournier, Y. Zhang, Q. Bao, Y.-B. Cheng, L. Spiccia and U. Bach, Dipole-field-assisted charge extraction in metal-perovskite-metal back-contact solar cells, *Nat. Commun.*, 2017, **8**, 613.

33 J. J. Yoo, S. Wieghold, M. C. Sponseller, M. R. Chua, S. N. Bertram, N. T. P. Hartono, J. S. Tresback, E. C. Hansen, J.-P. Correa-Baena, V. Bulović, T. Buonassisi, S. S. Shin and M. G. Bawendi, An interface stabilized perovskite solar cell with high stabilized efficiency and low voltage loss, *Energy Environ. Sci.*, 2019, **12**, 2192–2199.

34 P. Lv, Y. Yang, N. Li, Y. Zhang, M. Hu, B. Huang, Y. Zhu, Y. Wang, J. Pan, S. Wang, B. Zhang, F. Huang, Y.-B. Cheng and J. Lu, Hypervalent potassium xanthate modified SnO_2 for highly efficient perovskite solar modules, *Chem. Eng. J.*, 2023, **456**, 140894.

35 Y. Mo, C. Wang, X. Zheng, P. Zhou, J. Li, X. Yu, K. Yang, X. Deng, H. Park, F. Huang and Y.-B. Cheng, Nitrogen-doped tin oxide electron transport layer for stable perovskite solar cells with efficiency over 23%, *Interdiscip. Mater.*, 2022, **1**, 309–315.

36 Y. Wang, Y. Yang, N. Li, M. Hu, S. R. Raga, Y. Jiang, C. Wang, X.-L. Zhang, M. Lira-Cantu, F. Huang, Y.-B. Cheng and J. Lu,

Ionic Liquid Stabilized Perovskite Solar Modules with Power Conversion Efficiency Exceeding 20%, *Adv. Funct. Mater.*, 2022, **32**, 2204396.

37 Y. Niu, D. He, X. Zhang, L. Hu and Y. Huang, Enhanced Perovskite Solar Cell Stability and Efficiency via Multi-Functional Quaternary Ammonium Bromide Passivation, *Adv. Mater. Interfaces*, 2023, **10**, 2201497.

38 R. J. E. Westbrook, T. J. Macdonald, W. Xu, L. Lanzetta, J. M. Marin-Beloqui, T. M. Clarke and S. A. Haque, Lewis Base Passivation Mediates Charge Transfer at Perovskite Heterojunctions, *J. Am. Chem. Soc.*, 2021, **143**, 12230–12243.

39 M. C. Schubert, L. E. Mundt, D. Walter, A. Fell and S. W. Glunz, Spatially Resolved Performance Analysis for Perovskite Solar Cells, *Adv. Energy Mater.*, 2020, **10**, 1904001.

40 X. Ma, J. Pan, Y. Wang, X. Gao, M. Hu, Z. Ku, Y. Ma, F. Huang, Y.-B. Cheng and J. Lu, Bromide complimented methylammonium-free wide bandgap perovskite solar modules with high efficiency and stability, *Chem. Eng. J.*, 2022, **445**, 136626.

41 S. Ravishankar, Z. Liu, U. Rau and T. Kirchartz, Multilayer Capacitances: How Selective Contacts Affect Capacitance Measurements of Perovskite Solar Cells, *PRX Energy*, 2022, **1**, 013003.

42 N. Ma, J. Jiang, G. Wang, D. Wang, Y. Zhang, Y. Wang, Y. Wang, Y. Ji, W. Wei and L. Shen, Stable Perovskite Solar Cells with Bulk-Mixed Electron Transport Layer by Multi-functional Defect Passivation, *ACS Appl. Mater. Interfaces*, 2021, **13**, 44401–44408.

43 Y.-C. Chang, K.-M. Lee, C.-C. Ting and C.-Y. Liu, Step-efficient access to new starburst hole-transport materials with carbazole end-groups for perovskite solar cells via direct C–H/C–Br coupling reactions, *Mater. Chem. Front.*, 2019, **3**, 2041–2045.

44 W. Song, L. Rakocevic, R. Thiruvallur Eachambadi, W. Qiu, J. P. Bastos, R. Gehlhaar, Y. Kuang, A. Hadipour, T. Aernouts and J. Poortmans, Improving the Morphology Stability of Spiro-OMeTAD Films for Enhanced Thermal Stability of Perovskite Solar Cells, *ACS Appl. Mater. Interfaces*, 2021, **13**, 44294–44301.

45 Y. Ren, M. Ren, X. Xie, J. Wang, Y. Cai, Y. Yuan, J. Zhang and P. Wang, A spiro-OMeTAD based semiconductor composite with over 100 °C glass transition temperature for durable perovskite solar cells, *Nano Energy*, 2021, **81**, 105655.

46 A. Barranco, M. C. Lopez-Santos, J. Idigoras, F. J. Aparicio, J. Obrero-Perez, V. Lopez-Flores, L. Contreras-Bernal, V. Rico, J. Ferrer, J. P. Espinos, A. Borras, J. A. Anta and J. R. Sanchez-Valencia, Enhanced Stability of Perovskite Solar Cells Incorporating Dopant-Free Crystalline Spiro-OMeTAD Layers by Vacuum Sublimation, *Adv. Energy Mater.*, 2020, **10**, 1901524.